IEEE Access
Multidisciplinary | Rapid Review | Open Access Journal

Received 27 July 2024, accepted 18 August 2024, date of publication 22 August 2024, date of current version 2 September 2024.

Digital Object Identifier 10.1109/ACCESS.2024.3448219

RESEARCH ARTICLE

Advancing Ovarian Cancer Diagnosis Through Deep Learning and eXplainable AI: A Multiclassification Approach

MEERA RADHAKRISHNAN[1], NIRANJANA SAMPATHILA[1], (Senior Member, IEEE), H. MURALIKRISHNA[2], AND K. S. SWATHI[3]

[1]Department of Biomedical Engineering, Manipal Institute of Technology, Manipal Academy of Higher Education, Manipal 576104, India
[2]Department of Electronics and Communication Engineering, Manipal Institute of Technology, Manipal Academy of Higher Education, Manipal 576104, India
[3]Department of Social and Health Innovation, Prasanna School of Public Health, Manipal Academy of Higher Education, Manipal 576104, India

Corresponding authors: Niranjana Sampathila (niranjana.s@manipal.edu) and H. Muralikrishna (murali.h@manipal.edu)

ABSTRACT Ovarian cancer is a dangerous gynaecological malignancy, and the presence of many subtypes causes significant diagnostic difficulties. In general, the high accuracy of classification results in adequate prognosis and effectiveness of treatment. This work aims at the development of a Deep Learning (DL) approach for subtypes of ovarian cancer multiclassification, which tries to solve the problem of the creation of precise and reliable diagnostic methods. In the work, we have used and explored various DL models such as MobileNetV2, VGG19, ResNet18, ResNeXt, Xception, EfficientNet, and InceptionV3 to perform the classification task. Further, we used the state-of-the-art eXplainable Artificial Intelligence methods, including integrated gradient, saliency map, Grad-CAM, and DeepLift, to improve model interpretability. From our experiments, we inferred that the highest accuracy was achieved by InceptionV3, with a value of 97.96%. XAI techniques incorporated provide transparent insights into the model's operations during the decision-making process, thus increasing the level of trust and clinical usability. The proposed DL approach, by leveraging InceptionV3 as its top performer, has convincingly demonstrated the potential of AI to revolutionize the diagnosis of ovarian cancer through a high level of accuracy in subtype classification. XAI techniques integrated allow transparency support for the model and further enable its clinical adoption. All of these developments have significant potential for improved patient outcomes within the scope of personalized medicine in ovarian cancer treatment.

INDEX TERMS Deep learning, digital pathology, multiclassification, ovarian cancer, XAI.

I. INTRODUCTION

As a carcinoma that ranks sixth in women diagnosed globally, ovarian cancer is a severe health concern. It is a significant contributor that affect women's reproductive system, accounting for around 4% of all occurrences of female cancer. Additionally, ovarian cancer stands as one of the most prominent gynaecologic carcinomas, trailing only uterine corpus cancer, yet surpasses all other female reproductive system cancers in annual mortality rate [1]. In 2020 alone, there were almost 0.3 million cases reported worldwide, leading to about 0.2 million deaths. Despite these concerning statistics, there is some grounds for optimism because over 0.8 million women live longer than five years following their diagnosis [2]. This survival rate is consistent with the disease's preliminary forecast.

It is anticipated that by 2040, there will be 0.4 million more newly diagnosed cases annually, and correspondingly mortality rates are expected to increase [2]. This is still a concern projected for the upcoming years. The barrier to the initial stages of ovarian cancer screening is because of its asymptomatic behaviour. To mitigate the global impact of ovarian cancer, this emphasizes the critical need for efficient prevention, early detection, and treatment techniques.

The associate editor coordinating the review of this manuscript and approving it for publication was Mohammad Zia Ur Rahman.

The heterogeneous behaviour of ovarian cancer, in which malignant tumours can grow from a range of diverse kinds of cells, such as epithelial cells, stromal or germ cells, accounts for its complexity [3]. The histotype of epithelial ovarian cancer, which is something of significant attention in epidemiological research, includes serous, endometrioid, clear cell, and mucinous subtypes. Figure 1 shows the categorisation of different types of epithelial ovarian cancer: 3% Mucinous type, 10% for Clear cell and Endometroid each and the highest class among all is Serous 70% to 80% [3], [4]. Furthermore, the management and classification of diseases are made more difficult by the existence of low-malignant potential or borderline tumours within these categories.

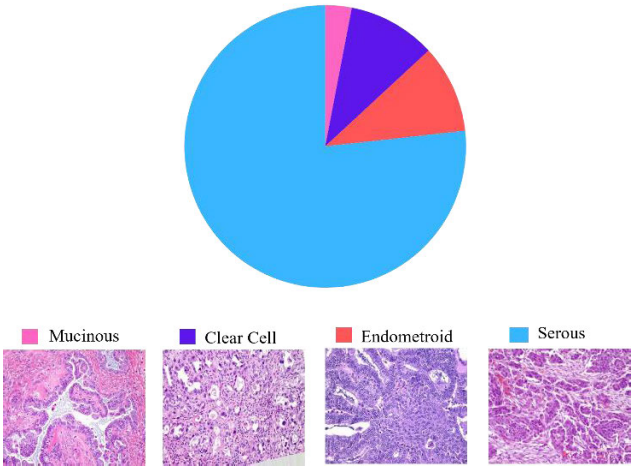

FIGURE 1. Ovarian cancer classification.

Early detection of ovarian cancer remains challenging due to the absence of known pre-malignant lesions and standardized screening tools, compounded by unresolved etiology compared to other cancers. This underscores the importance of ongoing research to elucidate risk factors and mechanisms of disease progression [5]. Pathological assessment of surgical resection specimens significantly impacts clinical care for endometrial cancer patients, yet inconsistencies persist at both macroscopic and microscopic levels, highlighting diagnostic and classification challenges [6]. Furthermore, the lack of a standard screening procedure makes the problem worse, increasing the likelihood of late-stage diagnosis and, eventually, worse patient outcomes. Improving the clinical management and prognosis of people with endometrial cancer requires addressing these issues.

The traditional approach for diagnosing ovarian cancer is transvaginal ultrasound (TVU), either alone or combined with CA-125. CA-125 (a serum tumour marker) is a protein that can be elevated in the blood of patients with ovarian cancer and other conditions. However, TVU and CA-125 do not provide the accuracy and precision needed for reliable early detection or timely assessment [7]. MRI is preferred for identifying ovarian cancer recurrence in the pelvic cavity and challenging-to-evaluate areas like the bladder and vagina, surpassing ultrasound, and CT scans [8]. But these imaging techniques themselves will not suffice the need for timely detection and assessment or effective management of recurrence of this disease in patients.

A. ADVANCES IN DEEP LEARNING ARCHITECTURES FOR MEDICAL IMAGING

The medical imaging profession has advanced significantly in the past few years, especially with the introduction of large-scale data and AI [9]. DL, a subset of AI, has transformed the analysis of medical images by enabling automated feature extraction ensuring rapid decision making for medical professionals [9]. It learns patterns and features from data through iterative training, adjusting connections between neurons to improve accuracy based on labelled data [10]. DL models analyse medical images from various modalities like X-rays, CT scans, MRI, and histopathological slides, aiding in the detection of abnormalities, disease classification, and organ or lesion segmentation. Specifically, AI applications in ovarian carcinoma imaging offer potential for improved tumour characterization and early diagnosis.

The widespread adoption of convolutional neural networks (CNNs), a type of DL model, has transformed various fields, including natural language processing (NLP), computer vision, and medical imaging. CNNs excel in analysing visual data by autonomously learning nested structures directly from raw input data. In medical imaging, CNNs have found extensive use in tasks like anomaly detection, identifying anatomical structures, and predicting patient outcomes. For instance, in radiology, CNNs assist radiologists by pinpointing areas of interest, detecting subtle irregularities, and providing quantitative assessments from imaging studies [11], [12]. Furthermore, in pathology, CNNs excel at identifying cancerous cells and classifying tissue types, aided by large, labelled datasets and computational advancements, enabling seamless adaptation to new tasks.

Specialized architectures like ResNets [13], inception networks, and attention mechanisms have enhanced CNNs' ability to handle complex visual data. ResNets, for example, introduce shortcut connections to address training complexity, mitigating issues like the vanishing gradient. VGG19 [13], developed by the Visual Geometry Group, employs small convolutional filters and max-pooling layers, proving effective in image classification tasks and serving as a benchmark model in DL evaluations. MobileNetV2 [14], designed for embedded and mobile devices, utilizes depth-wise separable convolutions to maintain accuracy while minimizing computational costs. This architecture achieves impressive results in tasks such as object recognition and image categorization, making it suitable for resource-constrained environments. Part of the Inception family, InceptionV3 [15] has an efficient feature extraction capability at many scales attributable to its multi-branch design and inception modules. Its ability to capture diverse features across different spatial resolutions makes it particularly well-suited for complex

visual recognition tasks. Xception [16], short for ''Extreme Inception,'' is also a CNN architecture. It is inspired by the Inception architecture but replaces standard convolutions with depth wise separable convolutions. This modification aims to capture both spatial and channel-wise dependencies more efficiently. Xception achieves competitive performance with significantly fewer parameters compared to traditional CNNs, making it suitable for resource-constrained environments. Cardinality is introduced by ResNeXt50 [17], an expansion of the ResNet architecture, which aggregates feature maps from multiple paths to expand model capacity and improve performance. By leveraging the cardinality mechanism, ResNeXt50 achieves better utilization of model parameters and enhanced representation learning capabilities. Another CNN architecture, EfficientNet [18] utilizes compound scaling to optimize model size, resolution, and depth concurrently, resulting in improved performance across different computational budgets. This approach ensures a balanced trade-off between computational cost and accuracy, rendering EfficientNet suitable for real-world applications.

B. ENHANCING DEEP LEARNING MODELS FOR MEDICAL IMAGING WITH EXPLAINABLE AI (XAI)

After exploring DL models, the importance of XAI [19] becomes apparent. XAI techniques [19] help unravel the reasoning behind complex model predictions, enhancing trust and facilitating their effective use, particularly in healthcare. By unravelling the DL models' ''black box'' feature, XAI not only enhances their interpretability but also facilitates the identification of potential biases or errors, thus fostering greater trust and acceptance in AI systems [20]. Figure 2 explains how XAI unravels the black box, providing interpretation and explanation to the end user.

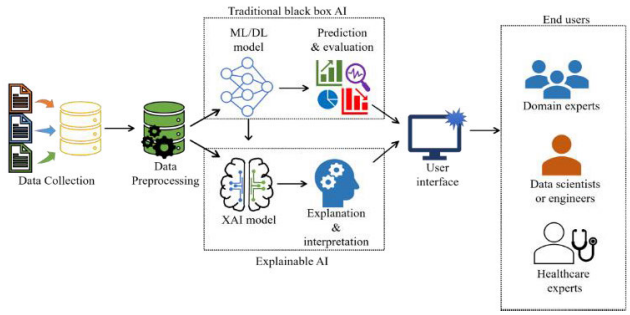

FIGURE 2. Transparency through XAI.

In medical imaging, XAI plays a crucial role in ensuring transparency and accountability of DL models, aiding in precise diagnoses. Techniques like saliency maps and gradient-based methods visualize key image regions, providing valuable insights to clinicians. Integrating XAI into DL models is essential for advancing transparency and trustworthiness in AI systems, ensuring they are not only accurate but also comprehensible and accountable.

There are very few state-of-the-art studies in Subtype Prediction (STEP) for ovarian cancer that perform comprehensive evaluations on model relevance and performance. The existing literature is heavily dominated by single-model investigations, and no analysis comparing different DL structures has been done. In addition, most works do not use explainable AI techniques to explain the models' interpretability and reliability, which is important for clinical acceptance.

This study addresses three primary research questions: First, as the traditional approach do not provide a reliable early detection, can DL models accurately classify subtypes of ovarian cancer using medical imaging data with greater accuracy and precision? Second, can experimenting on different DL model achieve the highest accuracy in multiclassification of ovarian cancer subtypes? Third, can one use XAI techniques to enhance the interpretability and trustworthiness of DL models in ovarian cancer diagnosis? The proposed method combines advanced DL models and XAI techniques to enhance ovarian cancer diagnosis. A detailed comparison with the existing studies is included in the discussion section.

Our study introduces several novel contributions to the field of ovarian cancer diagnosis using DL. This research aims to revolutionize ovarian cancer diagnosis, potentially leading to personalized treatment strategies and improved patient outcomes. This paper is organized into five sections, each aimed at making a specific contribution to the presentation of the research findings. Section II contains a comprehensive literature review detailing what is currently known and past research on classification of ovarian cancer using DL and also on the recent studies on XAI technique. Section III describes the proposed methodologies: the novel approaches applied in addressing the research questions. The section has focused on the exploration of seven DL models for a comparative analysis. The fourth section describes the experimental procedures and demonstrates results for crucial evaluation of the models using different metrics, then optimal DL model is selected for further interpretation using XAI. Discussion on the findings, arrival at the conclusions from our research, and a direction of how to carry future research will be suggested in Section V and VI.

II. RELATED WORK

Histopathology and medical imaging are crucial for diagnosing ovarian cancer, yet late-stage detection persists due to subtle symptoms and limited screening methods [21] for the disease in the general population. Late-stage ovarian cancer presents challenges including increased metastasis, aggressive tumour growth, and reduced treatment efficacy, underscoring the urgency for early detection and intervention [22]. Early ovarian cancer detection is crucial for better outcomes. AI and molecular profiling show promise in improving diagnostic accuracy and efficiency [23]. These developments have caused interest in using DL models to optimize ovarian carcinoma examination, especially with the

growing availability of large-scale datasets and computational resources.

Recent studies underscore the transformative potential of DL models in diagnosing and categorizing ovarian cancer, offering a paradigm shift in medical imaging interpretation. These models excel in deciphering complex patterns from extensive datasets, streamlining diagnostic imaging processes in resource-constrained healthcare settings [24]. Previous DL research in medical imaging has shown substantial advancements, particularly with convolutional neural networks (CNNs), effectively interpreting medical images and assisting clinicians in decision-making. Gao et al. [25], detected ovarian carcinoma using ultrasound images of pelvic, using a DCNN model which surpassed radiologists in detection, achieving an average accuracy rate of 0.876. However, the DCNN model is limited by its retrospective nature, unbalanced image distribution, inconsistent empirical validations due to dataset limitations. Another research where CNN model was trained and tested on MRI images, including T2WI, DWI, ADC map, and CE-T1WI, for diagnosing both ovarian cancer and borderline tumours. With sensitivity ranging from 0.77 to 0.85, specificity from 0.77 to 0.92, accuracy from 0.81 to 0.87, and AUC from 0.83 to 0.89, CNNs exhibited diagnostic performance comparable to experienced radiologists, with the highest performance observed on the ADC map. The study's limitations include individual sequence evaluation rather than comprehensive multi-sequence diagnosis, and the need for more training images and integration of clinical data for improved model performance [26]. A radiomic and machine learning model was developed and evaluated by Chiappa et al. [27], using ultrasound images to predict ovarian mass malignancy risk. Three homogeneous groups (solid, cystic, motley) were analysed, achieving accuracies of 80%, 87%, and 81%, sensitivities of 78%, 75%, and 81%, specificities of 83%, 90%, and 81%, and AUCs of 87%, 88%, and 89%, respectively. The study's main weakness is its retrospective, single centre design and limited sample size for certain lesions. In the study [28], author utilized multimodal MRI and a technique for multiple instances learning to distinguish between the borderline and malignant epithelial ovarian tumours. MAC-Net achieved superior performance with an AUC of 0.878, forming a valuable measurement for medical differentiation.

A DL algorithm using convolutional neural networks was developed using routine MR imaging to distinguish between cancerous and benign ovarian tumours in [29]. The entire ensemble model, incorporating clinical factors and magnetic resonance imaging, exhibited increased precision (0.87 versus 0.64) and specificity (0.92 vs 0.64) compared to junior radiologists, with similar sensitivity between 0.75 and 0.63. The ensemble model utilized EfficientNet due to its superior speed and performance over ResNet. The study has limitations including selection bias, reliance on original pathology reports, recall concerns, limited data size. Christiansen et al. in [30] aimed to develop and assess a DNN-based ultrasound image processing system to distinguish benign from cancerous ovarian tumours, utilizing ResNet50, MobileNet, and VGG16 with transfer learning and ensemble modelling. The ensemble of DNNs estimated malignancy probability and classified tumours either as malignant/benign (Ovry-Dx1 model) or inconclusive/benign/cancerous (Ovry-Dx2 model). It achieved a sensitivity of 96.0%, comparable specificity to subjective assessment (86.7%), and, notably, Ovry-Dx2 exhibited a 93.7% specificity and 97.1% sensitivity, though with some lesions deemed inconclusive. The image quality homogeneity is one of the limitations of the study.

Employing demographic traits, serum markers, colour Doppler imaging in addition to morphological factors, Lu et al. [31] developed and analysed logistic regression and Multilayer Perceptron (MLP) algorithm which achieved an AUC of 0.954 in predicting ovarian tumour malignancy. The study employed 425 images (291 benign, 134 malignant) with a training set of 365 and a test set of 60, employing 7-fold cross-validation. Combining the white-box model to the existing methodology can make the model more promising. The study in [32] approached an accurate distinguish between images containing cancer cells and those without tumours, achieving AUCs exceeding 0.95 for AlexNet, GoogLeNet, and VGGNet are 0.955 ± 0.010, 0.974 ± 0.004, and 0.975 ± 0.001, respectively. Grad-CAMs verified that tumour cell clusters were given greater weights to distinguish cancerous cells from nearby benign tissue. They inspected 587 patients with recurrent serous ovarian adenocarcinomas; the approach combined proteomics, RNA-Seq, and whole-slide histopathology results. CNNs accurately determined carcinogenic areas (AUCs > 0.95) and categorized tumour grade with AUC greater than 0.80. Furthermore, the author demonstrated quantitative histopathology analysis, which effectively stratified patients based on how they responded to chemotherapy by employing platinum ($P = 0.003$). The limitation of the study lies in the dataset, the author mostly focused on the serous type of ovarian carcinoma, there is a need for extension in their approach in other types of epithelial ovarian carcinoma. Shin et al. in [33] made use of a large public image dataset from TCIA (The Cancer Image Archive) for 142 ovarian cancer patients to fine-tune Inception V3. External validation on 32 patients' pathology images was performed, enhancing classifier performance. Without style transfer, the corresponding AUROC and AUPRC values were 0.737 and 0.710, while after style transfer, they improved to 0.916 and 0.898. There is room for improvement in the performance and interpretability of the DL model using advanced method. 444 patients with high-grade serous ovarian cancer are included in a multivariate dataset, featuring pathology images stained with H&E and contrast-enhanced computed tomography scans is utilized, Boehm et al. [34] applied a CNN model (ResNet18) with an accuracy of 88%. The dataset included pathology images with four classes: tumour, stroma, fat, and necrosis. Integration of machine learning models for histology, radiology, and

clinicogenomic revealed complementary prognostic information, the researchers offered a promising approach for enhanced stratification of risks in carcinoma patients. Farahani et al. [35] proposed four DL networks were assessed for histotype classification of ovarian cancer through whole slide images stained with haematoxylin and eosin. Models included one-stage (VGG-19) and two-stage transfer learning algorithms, DeepMIL, and VarMIL. Performance was assessed on a training set of 948 slides and an independent test set of 60 patients. VGG-19 outperformed the other models, with an AUC of 0.959. The study in [36] demonstrated that NoisyEnsembles improved diagnostic accuracy on low-quality datasets, achieving 96.2% accuracy on high-quality tissue and 82.2% on low-quality tissue. There are few advancements in the adaption of XAI techniques as mentioned in the study [37] were they utilized GradCAM, GradCAM++, and Layerwise Relevance Propagation (LRP) as XAI techniques to interpret the decisions of a CNN model for cervical cell image classification. While GradCAM and GradCAM++ highlighted both nuclei and cytoplasm regions, LRP focused solely on the nuclei, considered the most relevant feature. In another research work, a computational model presents the classification of melanoma skin cancer images using CNNs and Vision Transformers (ViT). Both works utilized mask-guided techniques and specially designed segmentation modules in U2-Net to get the masks. An evaluation of this research is shown, with the use of Grad-CAM and Grad-CAM++ to provide the heatmaps for interpreting the model [38]. In study [39] a deep learning model is developed for the diagnosis of glaucoma using fundus images; its main components included segmentation by U-Net and ResNet50, while classification was further elaborated with a modified Inception V3. Heatmaps were generated using Grad-CAM and Grad-CAM++ for interpretability of the developed model. Another research work [40] showed that EnsembleCAM had the potential to improve interpretability in cervical cancer classification using pap smear images. In that manner, EnsembleCAM provided unified visual explanations through an ensemble of multiple Class Activation Maps with both GradCAM and Score-CAM. The utility on the model based on XceptionNet gained 89% accuracy while supporting effective localization of the nucleus, which was a key feature of malignancy in cervical cancer. In our proposed research work, we introduce a DL method for multiclassification of ovarian cancer subtypes, leveraging dataset augmentation and incorporating XAI techniques for enhanced accuracy and interpretability.

III. MATERIALS AND METHODS

A. DESCRIPTION OF DATASET

The dataset comprised 500 histopathological images (1430 × 550 PNG format), with approximately 100 images labelled for each subtype: Serous, mucinous, endometroid, non-cancerous and clear cell. Initially obtained from the National Cancer Institute's Genomic Data Commons (TCGA-OV repository), the GDC portal offered a comprehensive resource of high-quality images. It included more images, of the Serous subtype which contained 175 histopathological images, other subtypes are rare, with minimal available data. The dataset was chosen due to its extensive annotations by expert pathologists, ensuring relevance to ovarian cancer subtypes and no redundancy in the data. The dataset was used for training, analysis, and research as referenced in [41]. A validation dataset, constituting 10% of the complete dataset, was extracted and published on Mendeley Data by the authors. All images were meticulously categorized and labelled based on subtypes, ensuring dataset integrity.

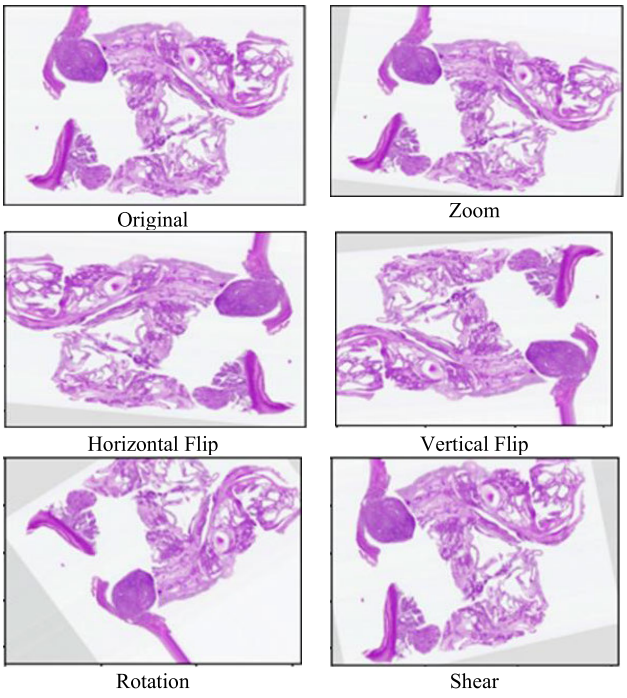

FIGURE 3. Image data augmentation.

B. DATA AUGMENTATION

For data preprocessing, image augmentation was performed which included rotation, shear, zoom, horizontal flip, and vertical flip. Each subtype's image directory was processed separately, generating augmented images to increase dataset diversity. The original dataset consisted of 500 histopathological images with 100 for clear cell, 100 for endometroid, 100 for mucinous, 100 for non-cancerous and 100 for serous. After augmentation it was 1,470 images across all five subtypes, with 295 images for clear cell, 286 for endometroid, 295 for mucinous, 297 for non-cancerous, and 297 for serous subtypes. The image dataset was resized, normalized, and converted to tensor according to each model requirement. The dataset was split into 70% and 30 % for training and validation set each respectively. This augmentation process enhances the dataset for robust model training and improves classification performance. Figure 3 depicts the different augmentation techniques used to increase the dataset for training.

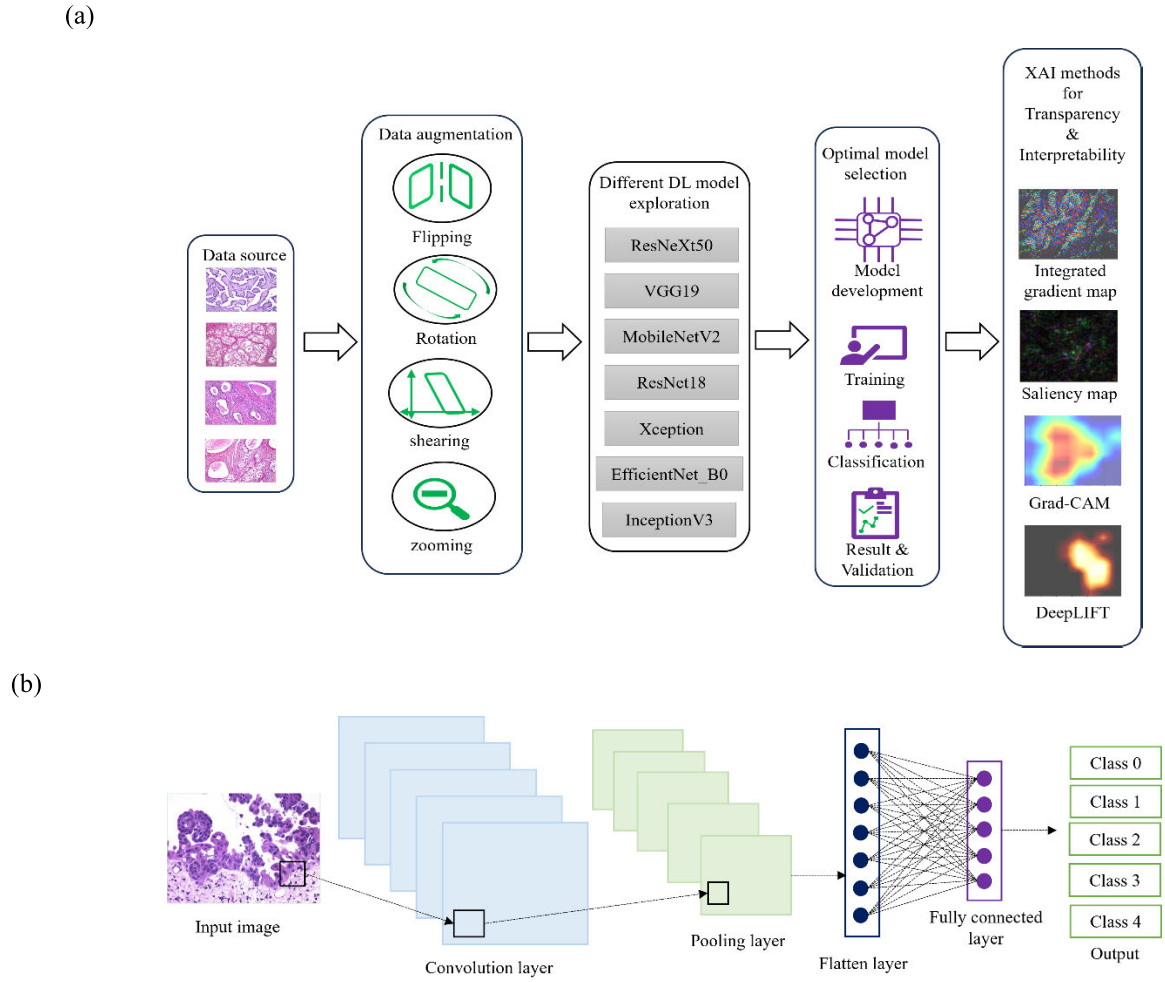

FIGURE 4. (a) Overview of proposed methodology and (b) architectural diagram of CNN model performing multi-classification task.

C. METHODOLOGY

Our methodology embarks on the utilization of a comprehensive dataset comprising histopathological images of ovarian cancer subtypes. To address potential data scarcity and enhance model robustness, we employed data augmentation techniques such as image rotation, flipping, zooming, and shearing. Subsequently, we explore a range of DL models, including MobileNetV2, VGG19, ResNet18, ResNeXt, Xception, EfficientNet, and InceptionV3, to determine their efficacy in classifying ovarian cancer subtypes. Among these models, InceptionV3 emerges as the top performer, demonstrating superior accuracy and generalization capabilities.

To ensure the interpretability and transparency of our AI-driven diagnostic tool, we integrate innovative XAI methods into our framework. These XAI techniques, including integrated gradient, saliency map, grad-cam, and DeepLift, provide insights into the decision-making process of the DL models. By making the reasoning behind the model predictions comprehensible to clinicians, our methodology aims to foster trust and acceptance of AI technologies in clinical settings. Figure 4 provides (a) an overview of the proposed methodology where it also describes the general workflow for the proposed work, the data collected from the source is augmented to increase the diversity then provided as input to the seven DL models. The optimal model is selected on the basis of different result and evaluation metrics and finally transparency and interpretability of the optimal model is experimented using different XAI techniques (b) an explanation of how CNN model is used to perform multi-classification task is explained with an architectural diagram of the model with the combination of convolutional, pooling, flatten and connected layer.

D. CLASSIFICATION MODELS

DL [42] has revolutionized machine learning with its ability to surpass human capabilities, particularly in CNNs, a DL subset, excel in image processing via convolutional layers, driving superior performance in classification tasks. Their versatility in healthcare spans disease detection, predictive analysis, and drug discovery, revolutionizing hospital workflows [43]. CNN methodologies evolved to handle diverse,

multi-class problems through refined processing units, optimized parameters, and redesigned layer patterns [44].

1) RESNEXT50

The first model used for training and classifying the ovarian carcinoma dataset was ResNeXt50 [45]. The OvarianCancerDataset class efficiently loaded images from a specified directory, assigning labels based on subdirectory names and enabling seamless iteration through the dataset. Data transformation, including resizing images to 224 × 224, conversion to tensors, and normalization, was applied using the defined transformation pipeline. Subsequently, the dataset was divided into 70% for training and rest for validation, followed by the initialization of DataLoader objects for both sets. These loaders facilitate efficient batched data loading during training, ensuring the smooth progression of model training and validation processes. The model's architecture was established, leveraging a pre-trained ResNeXt-50 backbone which includes 50 layers and a cardinality of 32 (number of groups), and a widening factor of 4, facilitating gradient flow and feature extraction. A fully connected layer serves as the classifier. The training loop iterates over epochs, updating gradients, applying regularization, and monitoring training and validation metrics. Upon completion, model evaluation assesses performance on unseen data, visualized through accuracy and loss curves. The flow chart of ResNeXt50 model architecture is given in Figure 5.

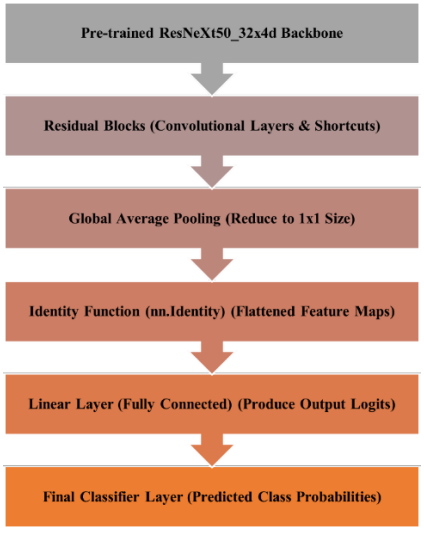

FIGURE 5. ResNeXt50 model architecture.

2) VGG19

The data loading, data transformation pipeline and initialization of DataLoader was similar for all the models. VGG19 [46], a widely recognized convolutional neural network (CNN) architecture is well known for being convenient to use and efficient for applications involving image classification. The model consists of several convolutional layers with a rectified linear unit (ReLU) activation function placed after each layer, designed to capture intricate patterns and features within input images. These convolutional layers are organized into distinct blocks, with each block comprising multiple convolutional layers and max-pooling layers, which function to decrease the feature maps' spatial dimensionality while preserving essential features. Following the convolutional layers, the model includes fully connected layers responsible for transforming the extracted high-level features into a vector of logits, representing the raw class scores for each class in the classification task. To prevent overfitting, the model incorporates weight decay regularization, which penalizes large weights during training to enhance generalization performance. Visualization tools plot accuracy and loss curves to monitor training progress. Finally, the performance of the model is assessed on the validation dataset, collecting predictions, true labels, and losses for further analysis. Figure 6 illustrates the model architecture of VGG19.

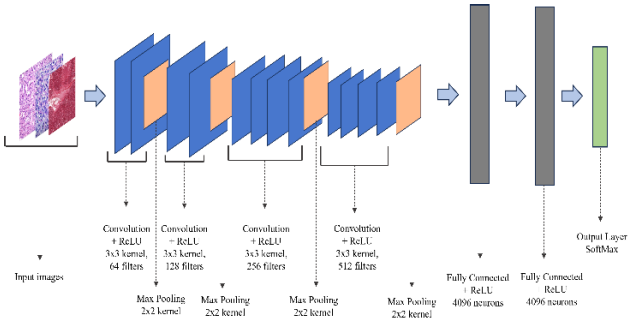

FIGURE 6. VGG19 model architecture.

3) MOBILENETV2

MobileNetV2 [47], a miniature convolutional neural network (CNN) intended for embedded and smartphone usage. For each input channel, Depthwise Convolution applies a single filter, capturing spatial correlations within channels, followed by Pointwise Convolution combines features across channels by using a 1 × 1 filter. Together, they form the Bottleneck layer in the model, reducing parameters and computational cost while maintaining expressive power. This configuration enhances the model's capacity by capturing both spatial and cross-channel correlations. After the bottleneck layer typically ReLU activation and batch normalization comes next. For the research work, the MobileNetV2 model is pretrained on the ImageNet dataset, allowing for transfer learning to adapt it to multiclassification task. The model classifier part is modified to accommodate the target dataset's class count, ensuring compatibility. Table 1 explains the architecture of MobileNetV2.

During training, the model undergoes an iterative optimization process using the Adam optimizer, aiming to reduce the loss of cross-entropy between the true and predicted labels. A validation dataset is used to assess the model to evaluate its performance. Accuracy and loss curves are plotted to visualize the training progress and monitor for signs of overfitting.

TABLE 1. MobileNetV2 architecture summary.

Layer Type	Output Size	Depth	Kernel Size/Stride	Activation
Input	224 x 224 x 3	-	-	-
Convolution	112 x 112 x 32	32	3x3	ReLU
Batch Normalization	112 x 112 x 32	32	-	-
Bottleneck	112 x 112 x 16	16	1x1, 3x3	ReLU
Bottleneck	112 x 112 x 24	24	1x1, 3x3	ReLU
Bottleneck	56 x 56 x 24	24	1x1, 3x3	ReLU
Bottleneck	56 x 56 x 32	32	1x1, 3x3	ReLU
Bottleneck	28 x 28 x 32	32	1x1, 3x3	ReLU
Bottleneck	28 x 28 x 64	64	1x1, 3x3	ReLU
Bottleneck	14 x 14 x 64	64	1x1, 3x3	ReLU
Bottleneck	14 x 14 x 96	96	1x1, 3x3	ReLU
Bottleneck	14 x 14 x 96	96	1x1, 3x3	ReLU
Bottleneck	7 x 7 x 160	160	1x1, 3x3	ReLU
Bottleneck	7 x 7 x 160	160	1x1, 3x3	ReLU
Bottleneck	7 x 7 x 320	320	1x1, 3x3	ReLU
Convolution	7 x 7 x 1280	1280	1x1	ReLU
Global Avg Pool	1 x 1 x 1280	-	Global	-
Fully Connected	1 x 1 x num_classes	-	-	SoftMax

4) RESNET18

Images are resized to 224×224 pixels and normalized to load and input to the ResNet18 model [48]. The model consists of a series of convolutional layers organized into residual blocks. To mitigate the vanishing gradient problem, each residual block has several layers of convolution in addition to identity shortcuts, or skip connections, that facilitate the gradient's flow during training. This architecture enables the training of deeper networks while maintaining computational efficiency. The number of cancer classifications to be predicted determines the total volume of outputs in the fully connected linear layer. Weight decay regularization is applied to the optimizer to prevent overfitting during training. The forward method takes an input tensor x representing the input image and passes it through the ResNet18 backbone. The output of the backbone, which is a feature tensor, is then passed through the linear classifier to produce the final output logits, which represent the predicted probabilities of the input image belonging to each cancer class. Metrics like precision, recall, and accuracy are calculated to assess the model's performance on unseen data. Figure 7 illustrates the ResNet18 model architecture in a flow chart.

5) XCEPTION

The Xception [49] architecture's capabilities for feature extraction and classification, augmented with weight decay regularization, is used to improve generalization performance. Depth-wise separable convolutions, which split the standard convolution into depth-wise and point-wise convolutions, are used by Xception to reduce computational complexity without compromising representational capability. During the forward pass, input images are passed through the Xception backbone, which extracts hierarchical features from the images. Then it is fed into the fully connected layer, which produces logits representing the class scores for each input image. The final output is obtained by applying a SoftMax function to the logits, producing the predicted probabilities for each class.

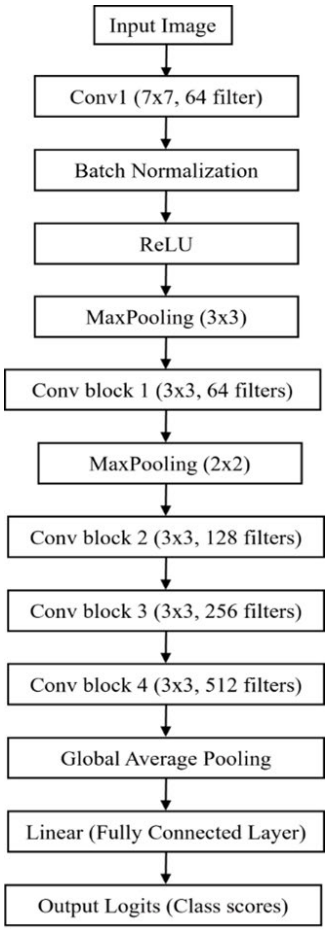

FIGURE 7. ResNet18 architecture.

The model summary is shown in Table 2. To avoid overfitting, early stopping is incorporated into the training loop. Training is terminated early if the validation loss remains unchanged after a certain number of epochs (patience). After training, the model is evaluated on the validation dataset to assess its performance.

TABLE 2. Xception architecture summary.

Layer (type)	Output Shape	Param #
Xception Backbone:		
Entry Flow:		
Conv2d-1	(16, 32, 112, 112)	896
BatchNorm2d-2	(16, 32, 112, 112)	64
ReLU-3	(16, 32, 112, 112)	0
Conv2d-4	(16, 64, 112, 112)	18,496
BatchNorm2d-5	(16, 64, 112, 112)	128
ReLU-6	(16, 64, 112, 112)	0
SeparableConv2d-7	(16, 128, 112, 112)	8,320
BatchNorm2d-8	(16, 128, 112, 112)	256
ReLU-9	(16, 128, 112, 112)	0
MaxPool2d-10	(16, 128, 56, 56)	0
Middle Flow (Repeated 8 times): Repeated modules from the Entry Flow multiple times		
Exit Flow:		
SeparableConv2d-45	(16, 1024, 7, 7)	2,082,304
BatchNorm2d-46	(16, 1024, 7, 7)	2,048
ReLU-47	(16, 1024, 7, 7)	0
Conv2d-48	(16, 1536, 7, 7)	1,572,864
BatchNorm2d-49	(16, 1536, 7, 7)	3,072
ReLU-50	(16, 1536, 7, 7)	0
Classifier Head:		
AdaptiveAvgPool2d-51	(16, 1536, 1, 1)	0
Flatten-52	(16, 1536)	0
Linear-53	(16, num_classes)	15,370
Total params: 20,865,530 Trainable params: 20,865,530 Non-trainable params: 0		

6) EFFICIENTNET-B0

EfficientNet-B0 [50] is known for its efficiency in terms of model size and computational cost while obtaining high precision. The pytorch library timm is used to initialize the model. The model architecture comprises a series of building blocks, including depthwise separable convolutions and squeeze-and-excitation (SE) blocks. These blocks efficiently extract features from input images while minimizing computational cost. The classifier head is responsible for producing the final predictions. The training loop iterates over the dataset for multiple epochs. The model is trained with the Adam optimizer and the cross-entropy loss function in each iteration. EfficientNet- B0 architecture is detailly explained in Figure 8.

7) INCEPTIONV3

The images were resized to meet the minimum size requirement of 299 × 299 pixels which is required for InceptionV3 model [51]. The neural network architecture model is designed for advanced classification tasks. The forward method delineates the model's forward pass, executing the sequential propagation of input tensors through the layers of the model. Figure 9 explains the model architecture. The integration of weight decay regularization into the optimizer further fortifies the model against overfitting tendencies by imposing penalties on large parameter values, thereby fostering a more robust and generalized model representation.

Essential components such as the loss function, optimizer, and scheduler, are initialized facilitating effective training management. The trained model is evaluated on the validation dataset, generating predictions to assess performance, while a confusion matrix aids in comprehensively analysing classification results.

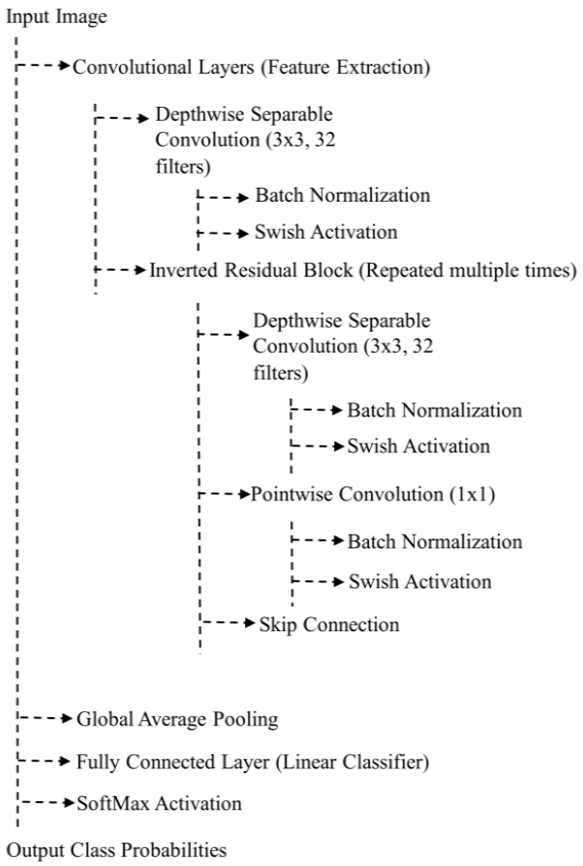

FIGURE 8. EfficientNet-B0 architecture.

The selection of the seven CNN models - MobileNetV2, VGG19, ResNet18, ResNeXt, Xception, EfficientNet, and InceptionV3 - for the comparative study in the proposed research work on ovarian cancer subtype classification is well-justified. This diverse set includes state-of-the-art models pre-trained on large datasets, enabling transfer learning capabilities. It covers a range of architectural approaches (residual connections, depth-wise separable convolutions, inception modules) and model complexities (from lightweight to deep and complex). This variety allows for a comprehensive evaluation of different architectural choices,

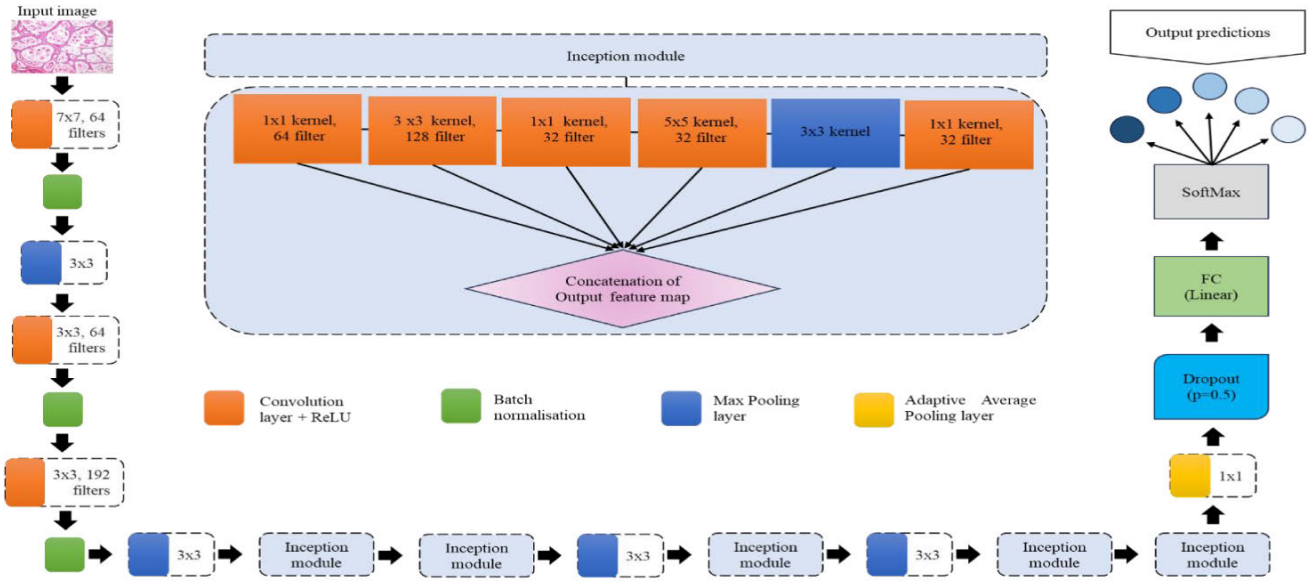

FIGURE 9. InceptionV3 architecture.

assessing the trade-off between model complexity and performance, and identifying the most suitable architecture for the critical task of accurate ovarian cancer subtype classification, which has significant implications for personalized medicine and clinical decision-making.

E. XAI TECHNIQUES

By employing XAI techniques, the research aims to enhance the interpretability and transparency of the DL models used for ovarian cancer subtype classification. XAI techniques, such as integrated gradient, saliency map, grad-cam, and DeepLift are employed [52].

1) INTEGRATED GRADIENT

Integrated gradient technique is one of the simplest approaches. It attributes the model's prediction to the input features by computing the integral of the gradients along a straight path from a baseline input to the actual input. This technique calculates the output of the target neuron at multiple points along the path, resulting in an importance score or attribution value for each input pixel. It highlights the regions of the input image that significantly influence the model's output.

2) SALIENCY MAP

Saliency maps visualize the pixels in the input image that contribute the most to the model's prediction. The DL model selects a target neuron from an input image, computes partial derivatives of its activation, and uses the absolute value to create a saliency map, highlighting the most significant input pixels. The saliency map is a heat map overlaid on an input image, with warmer colours indicating pixels with higher influence on the model's target class prediction.

3) GRAD-CAM

Grad-CAM is a visualization technique that uses gradients to identify important regions in an input image that significantly influence the prediction of a specific class. It computes gradients of the target class score and importance weights for each feature map, which are then used to compute a coarse localization map. Grad-CAM's unique feature is that it doesn't require architectural changes or re-training, making it widely applicable to any CNN-based model.

4) DEEPLIFT

DeepLIFT is a DL approach that uses a reference input as a baseline for comparison. It propagates the reference input through the neural network, computes and stores the activations of hidden units, and performs a backward pass. It employs specific rules for attributing relevance scores to input features, such as the Rescale Rule and RevealCancel Rule. By computing an attribution score for each input feature, DeepLIFT helps researchers understand the importance of different regions in the input tissue sample, building trust in DL models and facilitating their adoption in clinical settings.

The explanations are visual and measure the importance of input features, which can help to understand the model decision making. Such a framework also meets the pressing demand for interpretability of medical AI applications, which in turn will help to create trust, and drive the responsible deployment of these models into the clinic, to assist with the diagnosis or guide the next treatment options in the personalized care of ovarian cancer.

IV. RESULTS

In the study, several DL models were employed to classify ovarian cancer histopathology images, each yielding distinct

TABLE 3. Comparative analysis of ovarian cancer classification models.

MODELS		ResNeXt50	VGG19	MobileNetV2	ResNet18	Xception	EfficientNet_B0	InceptionV3
Overall accuracy		92.06%	93.65	95.46%	96.60%	97.05%	97.51%	97.96%
CLASS 0 (Clear Cell)	Precision	0.87	0.94	0.90	0.94	0.92	1.00	0.98
	Recall	0.96	0.94	0.95	0.98	1.00	0.98	0.97
	F1 score	0.91	0.94	0.92	0.96	0.96	0.99	0.97
CLASS 1 (Endometroid)	Precision	0.95	1.00	1.00	1.00	1.00	0.94	0.98
	Recall	0.99	0.95	1.00	0.99	1.00	0.97	0.99
	F1 score	0.97	0.98	1.00	1.00	1.00	0.95	0.98
CLASS 2 (Mucinous)	Precision	0.91	0.89	0.97	0.99	1.00	0.99	0.99
	Recall	0.83	0.91	0.95	0.92	0.89	0.94	0.97
	F1 score	0.86	0.90	0.96	0.95	0.94	0.96	0.98
CLASS 3 (Non-cancerous)	Precision	0.90	0.91	0.91	0.91	0.93	0.95	0.99
	Recall	0.92	0.95	0.97	0.98	0.99	1.00	0.99
	F1 score	0.91	0.93	0.93	0.94	0.96	0.98	0.99
CLASS 4 (Serous)	Precision	0.99	0.96	1.00	0.99	1.00	1.00	0.97
	Recall	0.90	0.94	0.91	0.96	0.98	1.00	0.98
	F1 score	0.94	0.95	0.95	0.98	0.99	1.00	0.97

accuracies. The ResNeXt50 model achieved an accuracy of 92.06%, followed by VGG19 with 93.65%, MobileNetV2 with 95.46%, ResNet18 with 96.60%, Xception with 97.05%, EfficientNet_B0 with 97.51%, and InceptionV3 with the highest accuracy of 97.96%, demonstrating its superior performance compared to other models. Table 3 shows a tabular representation showing the precision, recall, and F1 scores for each ovarian cancer class across all models, with emphasis on highlighting InceptionV3's superior performance.

The reason Regularized Inception Model outperforms the original one is that it incorporates advanced techniques in regularization, hyperparameter tuning, and optimization of training methods. These methods bring better model generalization, enhance robustness, and achieve a model of superior accuracy across diverse datasets.

1) **Architectural Improvements:** The enhanced Inception model is embedded with advanced regularization techniques to check overfitting and improve generalization. The inclusion of L2 regularization (weight decay) directly into the optimizer equips the model to handle complex datasets and allows more reliable performance
2) **Advanced Training Methods (Hyperparameters):**
   - *Regularization and Optimization:* L2 regularization (weight decay) adds a penalty to the loss function; as a result, the algorithm is incentivized not to assign unnecessarily large values to model parameters. This addresses issues related to overfitting and, therefore, increases robustness.
   - *Scheduling the learning rate:* The implemented ReduceLROnPlateau scheduler adapts the learning rates based on validation loss and promotes more efficient training by adjusting the learning rate at model plateaus, thus accelerating the convergence and not allowing for premature saturation.
3) **Enhanced Loss Function:** The CrossEntropyLoss function is supplemented with the regularization term, aiding in further improving the model performance as it will include weight decay in the computation of loss. This helps in accuracy during classification and also helps attain better convergence at training time.
4) **Improved Training and Validation Accuracy:** The model avoids overfitting and, through early stopping and validation monitoring, guarantees that it increases or maintains its best performance all through the

(a)

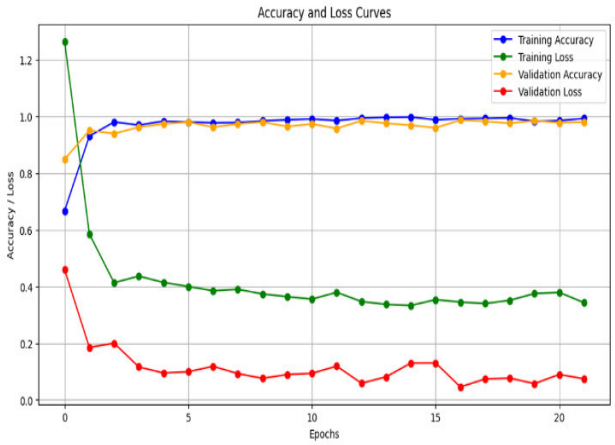

(b)

	Precision	Recall	Sensitivity	Specificity	F1 score	Support
Class 0	0.98	0.97	1.00	0.95	0.97	89
Class 1	0.98	0.99	0.98	1.00	0.98	82
Class 2	0.99	0.97	0.96	0.98	0.98	69
Class 3	0.99	0.99	1.00	0.99	0.99	102
Class 4	0.97	0.98	0.97	0.99	0.97	99
accuracy					0.98	441
macro avg	0.98	0.98	0.98	0.98	0.98	441
weighted avg	0.98	0.98	0.98	0.98	0.98	441

(c)

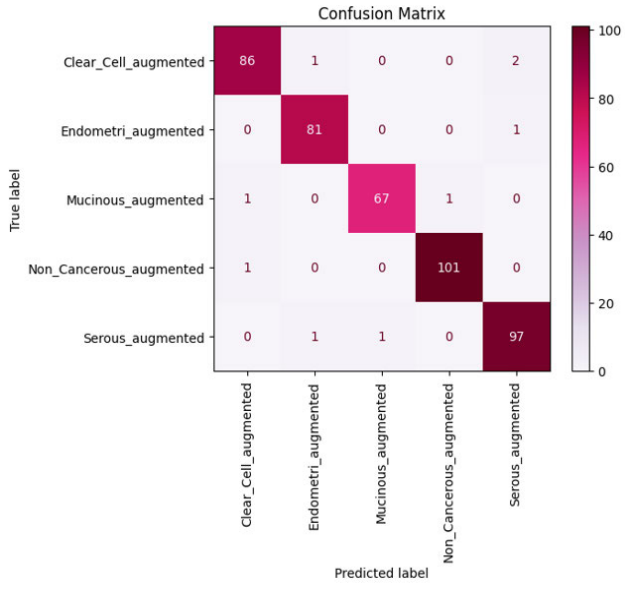

FIGURE 10. Evaluation of InceptionV3 model performance for ovarian cancer classification: (a) accuracy and loss curve plot, (b) classification report, and (c) confusion matrix.

training process. That is the reason it gets higher training accuracy and much higher validation accuracy than the baseline model.

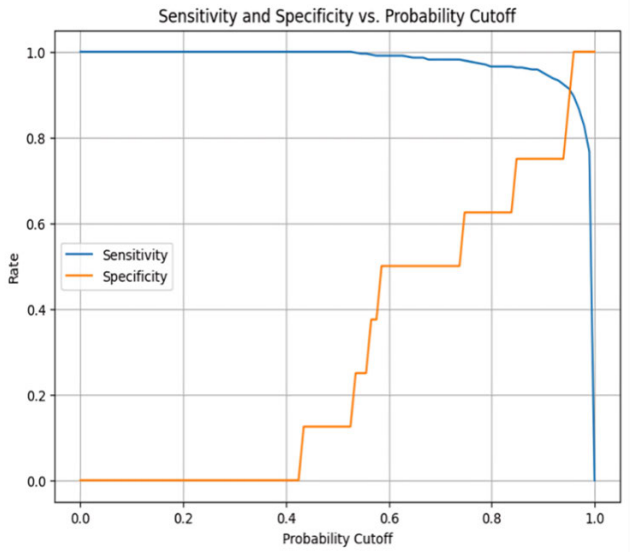

FIGURE 11. Threshold analysis for sensitivity and specificity evaluation.

ResNeXt50 achieves high precision scores in Class 1 (Endometroid) and Class 4 (Serous), indicating its capability to correctly identify instances of these ovarian cancer subtypes, it exhibits lower precision in Class 2 (Mucinous) and Class 3 (Non-cancerous). The recall scores for Class 2 (Mucinous) and Class 4 (Serous) are lower compared to other classes. F1 scores reflect a balanced measure of precision and recall, with lower value for Class 2 (Mucinous) compared to the other classes. VGG19 highlight impressive performance across most classes, with particularly high precision scores in Class 1 (Endometroid) and Class 4 (Serous). F1 scores are also high, indicating robust overall classification performance. While there are minor variations in precision and recall scores across different classes. MobileNetV2 demonstrates robust performance across most classes, particularly excelling in Class 1 (Endometroid) and Class 4 (Serous), where it achieves perfect precision and high recall values.

The model's overall precision and recall scores are high, resulting in robust F1 scores across all classes. However, there is a slight decrease in recall for Class 0 (Clear Cell). Excellent performance across all classes is achieved by ResNet18, with high recall, precision, and F1 scores demonstrating its efficacy in precisely classifying ovarian cancer subtypes. Notably, it demonstrates flawless precision in Class 1 (Endometroid) and Class 4 (Serous), suggesting minimal misclassification within these groups. Displaying high precision, recall, and F1 scores Xception model reflect its capability in accurately categorizing ovarian cancer subtypes. It achieves exceptional recall rates, ensuring comprehensive identification of relevant instances across all classes. EfficientNet_B0 model achieves impressive F1 scores across all classes, signifying a balance between precision and recall. Its robust performance in classifying cancerous and non-cancerous samples further highlights its efficacy as a reliable model

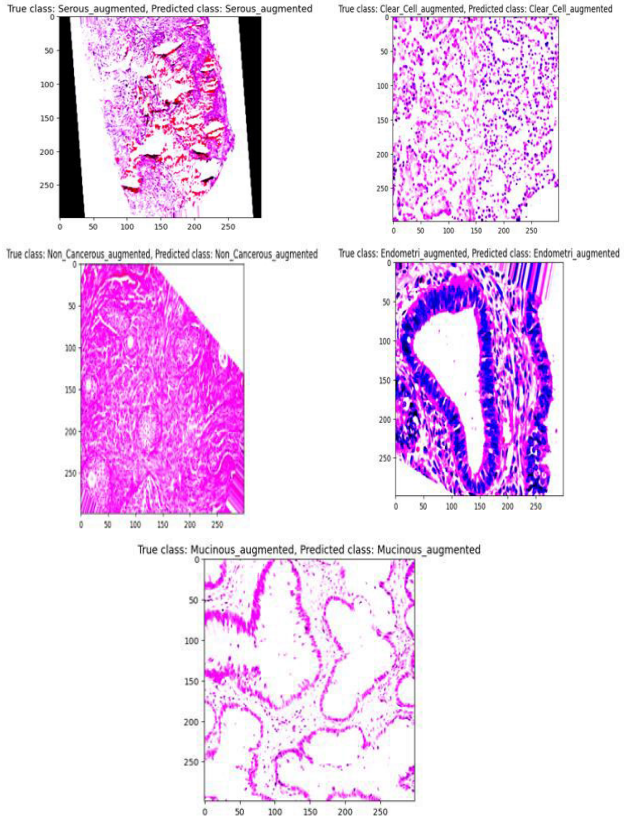

FIGURE 12. **Inference Outputs Comparison: Actual vs. Predicted class labels generated by the model.**

for subtype classification in ovarian cancer. InceptionV3 outperforms other models in classifying ovarian cancer subtypes with its high precision, recall, and F1 scores across all classes highlight its effectiveness in accurately identifying and distinguishing between different cancer subtypes. Particularly noteworthy is its precision and recall in Classes 1 (Endometroid), 2 (Mucinous), and 3 (Non-cancerous), where it achieves near-perfect scores, indicating minimal misclassification and comprehensive coverage of relevant instances. Additionally, a visualization of accuracy and loss curves to illustrate the training progression of the models is provided. Furthermore, a comprehensive analysis is presented, including classification reports and confusion matrices, offering insights into the models' classification performance and potential misclassifications. Figure 10 (a), (b), (c) shows accuracy and loss curve plots, classification report and confusion matrix, respectively.

The accuracy and loss curve plot explains the model's optimal performance, where the validation loss and accuracy curves draw into a steady converging state. The classification report provides a detailed explanation on precision, recall, specificity, sensitivity and F1 scores of each class. The accuracy of optimistic projections is reflected in precision, while recall measures the classifier's capability to recognize positive samples accurately. The F1-score balances precision and recall, making it suitable for imbalanced datasets.

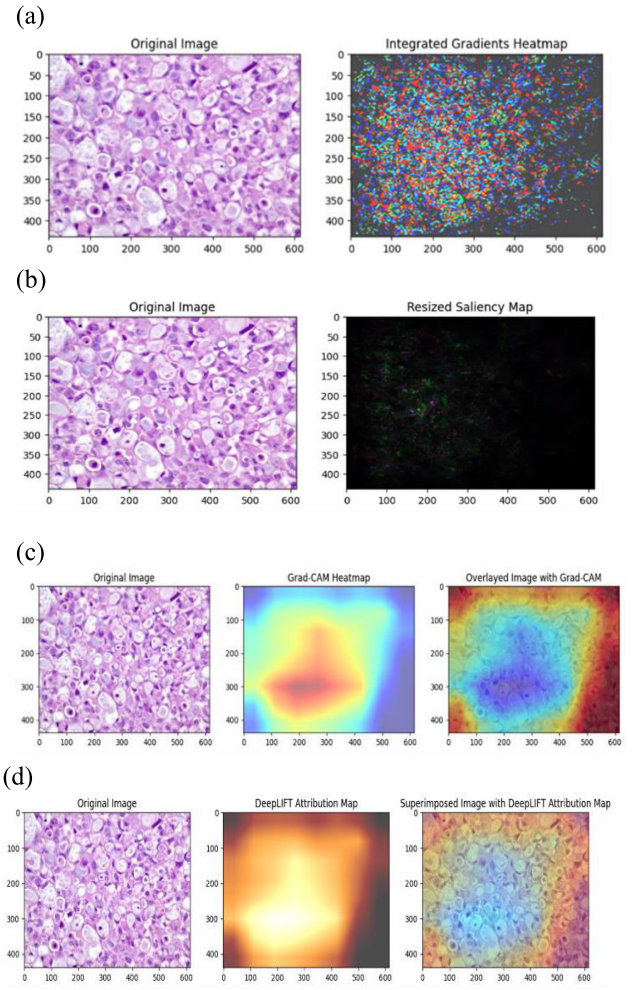

FIGURE 13. **XAI Integration with InceptionV3 model for Class 0 (Clear Cell) (a) integrated gradients, (b) saliency maps, (c) Grad-CAM and (d) DeepLift.**

Support indicates the number of each class's instances in the dataset, providing insights into class distribution and metric significance. A confusion matrix summarizes a classification model's performance by detailing the quantity of accurate and inaccurate predictions for each class, helping identify errors and biases. Analysing model performance across various probability thresholds involving the calculation of sensitivity (True Positive Rate) and specificity for different thresholds, sensitivity and specificity curve plot is displayed in Figure 11. Specificity shows the percentage of true negatives, whereas sensitivity measures the percentage of true positives. By iteratively adjusting the threshold and computing these metrics, the model's performance changes can be noted. Sensitivity and specificity trade-offs can be visualized to know the threshold selection, which is crucial for optimizing model performance based on specific task requirements.

Inference outputs are depicted in Figure 12, displaying the actual class labels alongside the predicted classes generated by the models, enabling a detailed examination of the model predictions. Figure 13 interprets the feature of Class 0 (Clear Cell). Different XAI methods are used to show

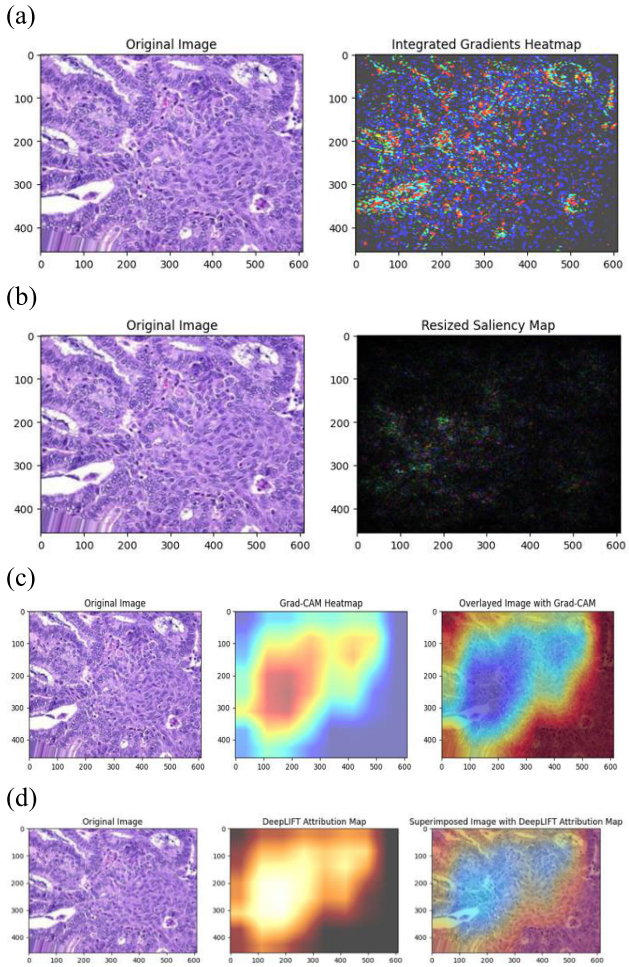

FIGURE 14. XAI Integration with InceptionV3 Model for Class 1 (Endometroid) (a) integrated gradients, (b) saliency maps, (c) Grad-CAM and (d) DeepLift.

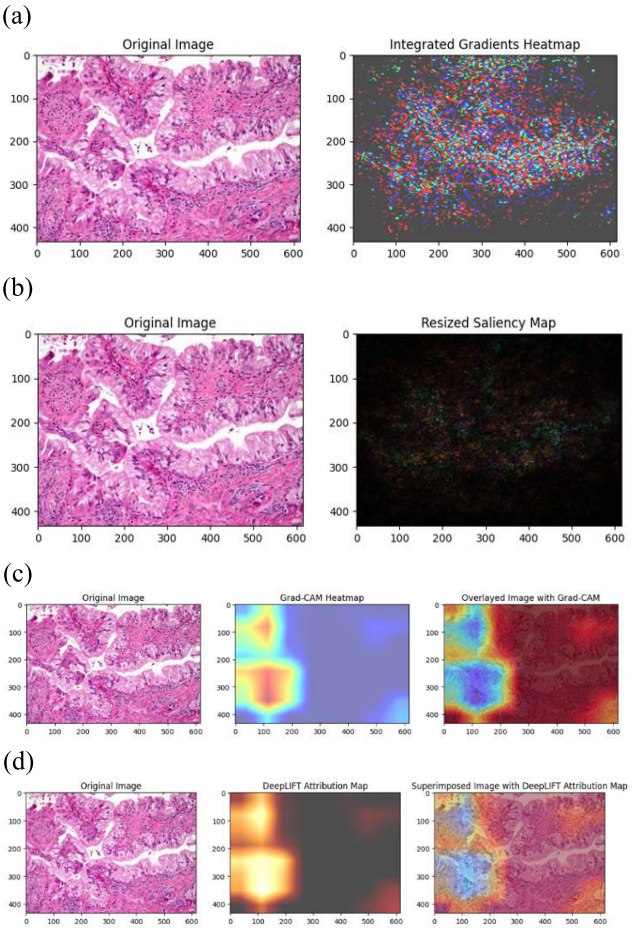

FIGURE 15. XAI Integration with InceptionV3 Model for Class 2 (Mucinous) (a) integrated gradients, (b) saliency maps, (c) Grad-CAM and (d) DeepLift.

the transparency of the InceptionV3 model. It includes the application of (a) Integrated gradients: A heatmap displays a colourful pattern where warmer colours (reds and yellows) indicate the areas that have a positive contribution to the prediction and cooler colours (blues and greens) present negatively contributing areas. From the heatmap we can see that the model is finding flattened clear cell regions to be highly significant features in identifying the Clear Cell subtype, (b) Saliency maps: the saliency map appears as a dark overlay on the original image, with brighter regions indicating higher relevance for the prediction. The saliency map highlights similar areas as the integrated gradients heatmap, (c) Grad-CAM: A broader tissue area, containing several flattened clear cells and the structures around them, is highlighted by heated hues (yellow and red) in the Grad-CAM heatmap, indicating that the model is considering the entire tissue pattern and morphological traits for classification, and (d) DeepLift: Cooler hues (blues) denote negative contributions, whereas warmer hues (reds and yellows) signify positive contributions. The original image has the attribution map superimposed on it for ease of interpretation. Class 1 (Endometroid)'s model predicted feature is shown in Figure 14. XAI methods (a) Integrated gradients: the heat map is highlighting the endometroid cell type regions with warmer hues (reds and yellows), and (b) Saliency maps: using the dark overlay for interpretability of the highly relevant features of the endometroid carcinoma class, (c) Grad-CAM: the attribution map is superimposed on the original image showing high significant feature in the grandular architecture, and (d) DeepLift: similar to Grad-CAM heated hues, indicate the explainability and transparency of the model. Integrated gradients, saliency maps, Grad-CAM, and DeepLift these methods are utilized in the next Class 2 (Mucinous) in Figure 15, where the model is predicting the tall columnar cells, with mucin filled cytoplasm differentiating it from other cell type classes. Figures 16 and 17 explain the XAI techniques used in the respective classes Class 3 (Non-Cancerous) and Class 4 (Serous). The XAI methods in the Non-Cancerous class type, has categorized this class from others by significantly marking the uniform, round nuclei without much variation in the size. And finally in Class 4 (Serous), the XAI techniques interprets and highlights the ciliated, clustered, or papillary projections of cell forming a solid mass like structure.

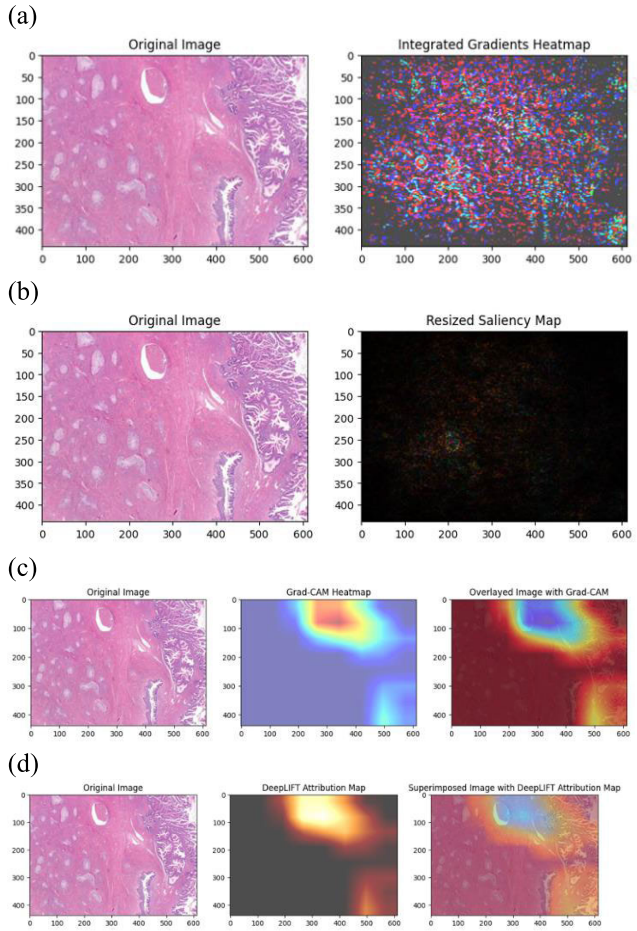

FIGURE 16. XAI Integration with InceptionV3 Model for Class 3 (Non-Cancerous) (a) integrated gradients, (b) saliency maps, (c) Grad-CAM and (d) DeepLift.

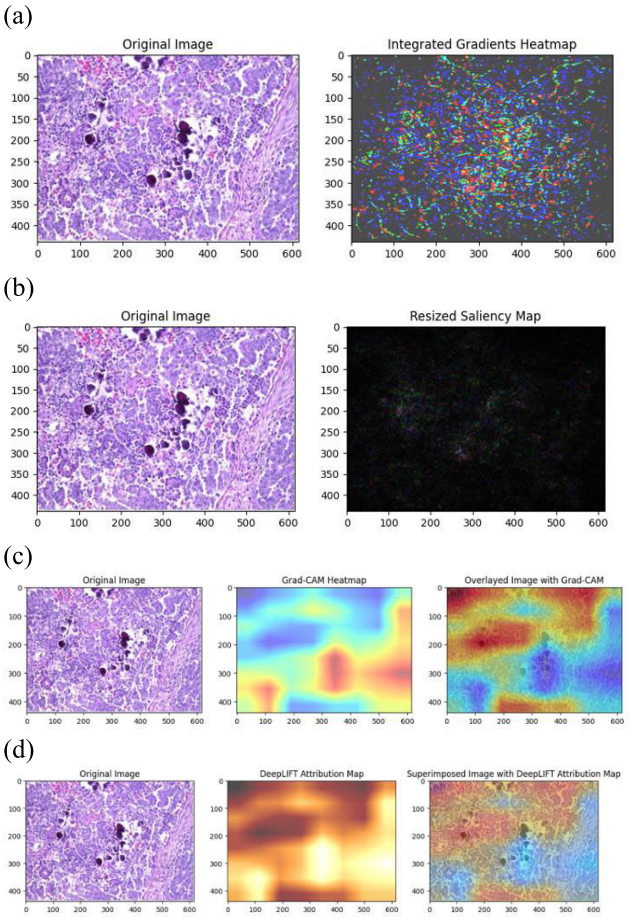

FIGURE 17. XAI Integration with InceptionV3 Model for Class 4 (Serous) (a) integrated gradients, (b) saliency maps, (c) Grad-CAM and (d) DeepLift.

Different histopathological subtypes of epithelial ovarian cancer are because of their distinct biological features [53], XAI provides visualization of these attributes which give a clarity about what exactly the model is learning. Each XAI technique refers to a method used for reflecting the InceptionV3 model's predictions.

V. DISCUSSIONS

Comparing other related studies is crucial for contextualizing the advancements and limitations of our proposed research work for diagnosing ovarian carcinoma subtypes. Understanding how existing approaches tackle similar challenges provides valuable insights into the efficacy and potential areas of improvement of our method. By critically evaluating the strengths and weaknesses of alternative methodologies, we can refine our approach. While achieving a commendable average accuracy of 91%, similar challenges provide valuable insights into the efficacy and potential areas of improvement of our method. By critically evaluating the strengths and weaknesses of alternative methodologies, we can refine our approach. While achieving a commendable average accuracy of 91%, the automatic system for diagnosing ovarian carcinoma subtypes in study [54] faces challenges in scalability and generalizability due to its testing on a limited dataset of 80 patients. The study also faces potential difficulty in clinically interpreting the complex features learned. In [55], BenTaieb et al. achieved a 95.0% multi-class classification accuracy for ovarian carcinoma subtypes by mimicking pathologists' workflow and using machine learning techniques on a small dataset. However, system performance may vary due to major reliance on high grade tumours for model development and validation. This may limit its generalizability to low grade or early-stage ovarian cancers, which are more common and often have different clinical characteristics.

In study 1 and 2, 80 slides from resection samples were analysed. The dataset is sourced from a prior trans-Canadian study [56] on ovarian cancer classification. Achieving 90% accuracy on a dataset of 133 patients, the histopathology-based approach in study [57] employs CNN and novel K-Means features with LSVM classification, demonstrating high accuracy and generality across feature types. This paper presents a learning algorithm simulating reasoning, and discriminative region highlighting for multi-magnification histopathology slide analysis. However, its robustness across diverse datasets needs further validation, particularly with additional learning methods. Authors

TABLE 4. Ovarian carcinoma classification: Methodological comparison.

Sr. No.	Study	Data modality	AI model	Metrics	Benefits	Limitations
1.	2015 [54]	histopathology (H&E)	multi-layer DN (CNN features); SVM - classifier	accuracy 91.0%	captured intricate tissue patterns, yielding robust features for ovarian cancer classification	applicability may be limited by the challenge of extrapolating results to larger datasets and difficulty in interpreting complex features.
2.	2016 [55]	histopathology (H&E)	SVM - classifier	accuracy 95.0%	demonstrates promising accuracy (95.0%) in subtype prediction	the system performance may vary due to reliance on high-grade tumours limits generalizability to low-grade or early-stage ovarian cancers.
3.	2017 [57]	histopathology (H&E)	features (CNN, novel K-Means); LSVM - classifier	accuracy 90%	demonstrates saliency map to identify the carcinoma	face challenges in interpretability and rely on specific image resolutions.
4.	2018 [58]	histopathology (H&E)	DCNN based on AlexNet	accuracy 78.20%	DCNN simplifies ovarian cancer classification, bypassing traditional segmentation and feature extraction steps.	sample diversity and complex morphology challenge DCNN accuracy, necessitating data expansion and model refinement.
5.	2020 [59]	histopathology (H&E)	GAN for synthetic image generation and VGG19 - classifier	AUC 0.9177	GANs provide synthetic images, ensuring consistent diagnostic system performance	insufficient training data for GANs may result in increased artifacts in synthetic images
6.	2021 [60]	histopathology (H&E)	DCNN	accuracy 83.93%	the DCNN model enhances prediction and classification accuracy	refinement is needed to address misclassifications and interpretability of model
7.	2022 [61]	histopathology (H&E)	ResNet18	AUC 0.97	Mixing colour normalization methods and reference images boosts AI diagnostic model robustness	The methods may complicate the diagnostic process.
8.	proposed work	histopathology (H&E)	InceptionV3	accuracy 97.96%	Our work achieves 97.96% accuracy, surpassing prior studies, and offers transparent model predictions using advanced XAI techniques.	-

in [58] utilized AlexNet, a Deep Convolutional Neural Network (DCNN), to enhance the classification accuracy of various ovarian cancer types from cytological images, achieving a notable improvement from 72.76% to 78.20% with augmented image data. The study collected 85 specimens stained with H&E from the First Affiliated Hospital of Xinjiang Medical University. The study is limited by the need for further investigation to address misclassifications, highlighting the necessity to increase the sample volume for refined model training. In study [59] GANs effectively replicate high-resolution pathology images, but limitations arise due to limited training data, leading to increased artifacts in synthetic images, especially in datasets with fewer samples, impacting image reliability. In the study [60], 500 labelled histopathological images were sourced from the National Cancer Institute's Genomic Data Commons data portal for training and analysis. The limitation lies in the modest accuracy achieved by the DCNN model suggesting the need for further refinement and optimization to enhance its predictive performance. Study [61] reviews eight colour normalization methods for AI-based histopathology slide classification with H&E staining, showing varied performance boosts in single-centre datasets. While a combined enhancement technique enhances diagnosis across external centres, it introduces complexity to diagnostic workflows. Archival tissue samples in study 5 and 6 were obtained from the BC Cancer Ovarian Care Research Program and Vancouver General Hospital pathology archive, digitized post institutional ethics board approval.

To address whether DL models can accurately classify subtypes of ovarian cancer, we implemented and evaluated a suite of DL models, including MobileNetV2, VGG19, ResNet18, ResNeXt, Xception, EfficientNet, and InceptionV3 in the proposed work. There is an absence of a separate test dataset which means that validation is relied on the 30% training split, which may affect the comprehensive evaluation of the model's performance. However, using dataset augmentation to enhance robustness, we trained and tested these models on labelled ovarian cancer imaging data, finding that DL models are capable of accurate classification, with InceptionV3 achieving the highest accuracy at 97.96% due to its superior feature extraction capabilities and multi-branch design. To improve interpretability and trustworthiness, we integrated Explainable AI (XAI) techniques, such as integrated gradient, saliency map, grad-cam, and DeepLift, providing visual explanations of the model's decision-making process and highlighting key image regions influencing predictions. This transparency facilitated the identification of potential biases or errors, enhancing clinician trust and supporting effective decision-making in clinical settings. Table 4

compares various methods for classifying ovarian carcinoma, highlighting differences in accuracy, methodology, and performance on diverse datasets.

VI. CONCLUSION AND FUTURE WORK

In conclusion, our research on ovarian cancer multiclassification utilizing DL models and XAI techniques has yielded remarkable results. By integrating dataset augmentation and exploring DL models like MobileNetV2, VGG19, ResNet18, ResNeXt, Xception, EfficientNet, and InceptionV3, we achieved a remarkable accuracy of 97.96%. Additionally, our pioneering use of XAI methods enhances model interpretability. The exceptional performance could be attributed to extensive dataset augmentation, meticulous hyperparameter tuning, and optimization of model architectures. This surpasses the performance of previous studies in the field, establishing a new benchmark for ovarian cancer classification accuracy.

Our study introduces a novel aspect by integrating advanced XAI techniques such as integrated gradient, saliency map, Grad-CAM, and DeepLift. These techniques provide transparent and interpretable visualizations of the model's predictions, enhancing the overall explainability of our approach. We promote trust and understanding among medical professionals and stakeholders by providing insights into the DL models' process of decision-making.

Moving forward, our findings hold significant implications for clinical practice and future research endeavours. We recommend integrating our high-performing DL models into clinical settings to aid pathologists in precise ovarian cancer subtype diagnosis. Various data augmentation techniques such as rotation, flipping, zooming, and shearing are employed. These augmentations create a more varied training set, helping the model to generalize better by simulating different imaging scenarios. The techniques and models employed are designed to be adaptable to other datasets. While the primary focus was on ovarian cancer subtype classification, the same approach can be extended to other types of medical imaging datasets. While the system is designed to support additional datasets, it has not yet been tested beyond those included in this study. Future work will involve testing and validating our model on additional datasets to further demonstrate its generalizability. Validating the model in clinical environments through pilot studies and real-world trials will be also involved. Collaborating with healthcare institutions, integrating the model into clinical workflows, and establishing continuous monitoring will be essential steps for clinical adoption. By conducting pilot studies and real-world trials in clinical settings, feedback will be sought from oncologists and radiologists to ensure the model's interpretability and accuracy. Moreover, further exploration in optimizing classification algorithms and leveraging advanced DL techniques could enhance diagnostic accuracy and robustness. Additionally, future work could focus on incorporating ensemble methods and expanding the application of XAI methods for classification tasks by using more diverse dataset to gain deeper insights into the underlying mechanisms of ovarian cancer pathology. These advancements have the potential to revolutionize ovarian cancer diagnosis and treatment through the seamless integration of DL and XAI technologies.

ACKNOWLEDGMENT

The authors would like to thank Manipal Academy of Higher Education for the research support.

REFERENCES

[1] M. Verma, *Cancer Epidemiology: Volume 2, Modifiable Factors*. Totowa, NJ, USA: Humana Press, 2008.
[2] M. Chaturvedi, S. Krishnan, P. Das, K. L. Sudarshan, S. Stephen, V. Monesh, and P. Mathur, "Descriptive epidemiology of ovarian cancers in India: A report from national cancer registry programme," *Indian J. Gynecologic Oncol.*, vol. 21, no. 1, p. 25, Mar. 2023.
[3] B. M. Reid, J. B. Permuth, and T. A. Sellers, "Epidemiology of ovarian cancer: A review," *Cancer Biol. Med.*, vol. 14, no. 1, p. 9, 2017.
[4] C. Stewart, C. Ralyea, and S. Lockwood, "Ovarian cancer: An integrated review," *Seminars Oncol. Nursing*, vol. 35, no. 2, pp. 151–156, Apr. 2019.
[5] N. Colombo, T. Van Gorp, G. Parma, F. Amant, G. Gatta, C. Sessa, and I. Vergote, "Ovarian cancer," *Crit. Rev. Oncol./Hematol.*, vol. 60, no. 2, pp. 159–179, 2006.
[6] G. Turashvili and K. Hanley, "Practical updates and diagnostic challenges in endometrial carcinoma," *Arch. Pathol. Lab. Med.*, vol. 148, no. 1, pp. 78–98, Jan. 2024.
[7] J. Zhou, W. Cao, L. Wang, Z. Pan, and Y. Fu, "Application of artificial intelligence in the diagnosis and prognostic prediction of ovarian cancer," *Comput. Biol. Med.*, vol. 146, Jul. 2022, Art. no. 105608.
[8] B. A. Saitkulovich, "Modern aspects of the use of magnetic resonance imaging in the diagnosis of ovarian cancer," *World Bull. Public Health*, vol. 30, pp. 63–66, Jan. 2024.
[9] M. Tsuneki, "Deep learning models in medical image analysis," *J. Oral Biosci.*, vol. 64, no. 3, pp. 312–320, 2022.
[10] Y. LeCun, Y. Bengio, and G. Hinton, "Deep learning," *Nature*, vol. 521, no. 7553, pp. 436–444, 2015.
[11] Z. Han, B. Wei, Y. Zheng, Y. Yin, K. Li, and S. Li, "Breast cancer multi-classification from histopathological images with structured deep learning model," *Sci. Rep.*, vol. 7, no. 1, p. 4172, Jun. 2017.
[12] H. H. Sultan, N. M. Salem, and W. Al-Atabany, "Multi-classification of brain tumor images using deep neural network," *IEEE Access*, vol. 7, pp. 69215–69225, 2019.
[13] R. Gabbasov and R. Paringer, "Influence of the receptive field size on accuracy and performance of a convolutional neural network," in *Proc. Int. Conf. Inf. Technol. Nanotechnol. (ITNT)*, May 2020, pp. 1–4.
[14] K. Dong, C. Zhou, Y. Ruan, and Y. Li, "MobileNetV2 model for image classification," in *Proc. 2nd Int. Conf. Inf. Technol. Comput. Appl. (ITCA)*, Dec. 2020, pp. 476–480.
[15] C. Wang, D. Chen, L. Hao, X. Liu, Y. Zeng, J. Chen, and G. Zhang, "Pulmonary image classification based on inception-v3 transfer learning model," *IEEE Access*, vol. 7, pp. 146533–146541, 2019.
[16] S. H. Kassani, P. H. Kassani, R. Khazaeinezhad, M. J. Wesolowski, K. A. Schneider, and R. Deters, "Diabetic retinopathy classification using a modified xception architecture," in *Proc. IEEE Int. Symp. Signal Process. Inf. Technol. (ISSPIT)*, Dec. 2019, pp. 1–6.
[17] H. Zhao, W. Zhou, X. Hou, and H. Zhu, "Double attention for multi-label image classification," *IEEE Access*, vol. 8, pp. 225539–225550, 2020.
[18] J. Wang, L. Yang, Z. Huo, W. He, and J. Luo, "Multi-label classification of fundus images with EfficientNet," *IEEE Access*, vol. 8, pp. 212499–212508, 2020.
[19] A. B. Arrieta, N. Díaz-Rodríguez, J. D. Ser, A. Bennetot, S. Tabik, A. Barbado, S. Garcia, S. Gil-Lopez, D. Molina, R. Benjamins, R. Chatila, and F. Herrera, "Explainable artificial intelligence (XAI): Concepts, taxonomies, opportunities and challenges toward responsible AI," *Inf. Fusion*, vol. 58, pp. 82–115, Jun. 2020.
[20] L. Famiglini, A. Campagner, M. Barandas, G. A. La Maida, E. Gallazzi, and F. Cabitza, "Evidence-based XAI: An empirical approach to design more effective and explainable decision support systems," *Comput. Biol. Med.*, vol. 170, Mar. 2024, Art. no. 108042.

[21] T. V. Gorodnova, A. P. Sokolenko, E. Kuligina, I. V. Berlev, and E. N. Imyanitov, "Principles of clinical management of ovarian cancer," *Chin. Clin. Oncol.*, vol. 7, no. 6, p. 56, Dec. 2018.

[22] Z. Nash and U. Menon, "Ovarian cancer screening: Current status and future directions," *Best Pract. Res. Clin. Obstetrics Gynaecol.*, vol. 65, pp. 32–45, May 2020.

[23] M. Akazawa and K. Hashimoto, "Artificial intelligence in gynecologic cancers: Current status and future challenges—A systematic review," *Artif. Intell. Med.*, vol. 10, no. 2, pp. 475–491, 2021.

[24] H. L. Xu, T. T. Gong, F. H. Liu, H. Y. Chen, Q. Xiao, Y. Hou, Y. Huang, H.-Z. Sun, Y. S. S. Gao, Y. Lou, Q. Chang, Y.-H. Zhao, Q.-L. Gao, and Q.-J. Wu, "Artificial intelligence performance in image-based ovarian cancer identification: A systematic review and meta-analysis," *eClinicalMedicine*, vol. 53, Nov. 2022, Art. no. 101662, doi: 10.1016/j.eclinm.2022.101662.

[25] Y. Gao et al., "Deep learning-enabled pelvic ultrasound images for accurate diagnosis of ovarian cancer in China: A retrospective, multicentre, diagnostic study," *Lancet Digital Health*, vol. 4, no. 3, pp. e179–e187, 2022, doi: 10.1016/S2589-7500(21)00278-8.

[26] T. Saida, K. Mori, S. Hoshiai, M. Sakai, A. Urushibara, T. Ishiguro, M. Minami, T. Satoh, and T. Nakajima, "Diagnosing ovarian cancer on MRI: A preliminary study comparing deep learning and radiologist assessments," *Cancers*, vol. 14, no. 4, p. 987, Feb. 2022, doi: 10.3390/cancers14040987.

[27] V. Chiappa, G. Bogani, M. Interlenghi, C. Salvatore, F. Bertolina, G. Sarpietro, M. Signorelli, I. Castiglioni, and F. Raspagliesi, "The adoption of radiomics and machine learning improves the diagnostic processes of women with ovarian masses (the AROMA pilot study)," *J. Ultrasound*, vol. 24, no. 4, pp. 429–437, Dec. 2021.

[28] J. Jian, W. Xia, R. Zhang, X. Zhao, J. Zhang, X. Wu, Y. Li, J. Qiang, and X. Gao, "Multiple instance convolutional neural network with modality-based attention and contextual multi-instance learning pooling layer for effective differentiation between borderline and malignant epithelial ovarian tumors," *Artif. Intell. Med.*, vol. 121, Nov. 2021, Art. no. 102194.

[29] R. Wang, Y. Cai, I. K. Lee, R. Hu, S. Purkayastha, I. Pan, T. Yi, T. M. L. Tran, S. Lu, T. Liu, K. Chang, R. Y. Huang, P. J. Zhang, Z. Zhang, E. Xiao, J. Wu, and H. X. Bai, "Evaluation of a convolutional neural network for ovarian tumor differentiation based on magnetic resonance imaging," *Eur. Radiol.*, vol. 31, no. 7, pp. 4960–4971, Jul. 2021.

[30] F. Christiansen, E. L. Epstein, E. Smedberg, M. Åkerlund, K. Smith, and E. Epstein, "Ultrasound image analysis using deep neural networks for discriminating between benign and malignant ovarian tumors: Comparison with expert subjective assessment," *Ultrasound Obstetrics Gynecol.*, vol. 57, no. 1, pp. 155–163, Jan. 2021.

[31] C. Lu, J. De Brabanter, S. Van Huffel, I. Vergote, and D. Timmerman, "Using artificial neural networks to predict malignancy of ovarian tumors," in *Proc. 23rd Annu. Int. Conf. IEEE Eng. Med. Biol. Soc.*, Oct. 2001, pp. 1637–1640.

[32] K.-H. Yu, V. Hu, F. Wang, U. A. Matulonis, G. L. Mutter, J. A. Golden, and I. S. Kohane, "Deciphering serous ovarian carcinoma histopathology and platinum response by convolutional neural networks," *BMC Med.*, vol. 18, no. 1, pp. 1–14, Dec. 2020.

[33] S. J. Shin, S. C. You, H. Jeon, J. W. Jung, M. H. An, R. W. Park, and J. Roh, "Style transfer strategy for developing a generalizable deep learning application in digital pathology," *Comput. Methods Programs Biomed.*, vol. 198, Jan. 2021, Art. no. 105815.

[34] K. M. Boehm et al., "Multimodal data integration using machine learning improves risk stratification of high-grade serous ovarian cancer," *Nature Cancer*, vol. 3, no. 6, pp. 723–733, Jun. 2022.

[35] H. Farahani, J. Boschman, D. Farnell, A. Darbandsari, A. Zhang, P. Ahmadvand, S. J. M. Jones, D. Huntsman, M. Köbel, C. B. Gilks, N. Singh, and A. Bashashati, "Deep learning-based histotype diagnosis of ovarian carcinoma whole-slide pathology images," *Modern Pathol.*, vol. 35, no. 12, pp. 1983–1990, Dec. 2022.

[36] R. S. Mayer, S. Gretser, L. E. Heckmann, P. K. Ziegler, B. Walter, H. Reis, K. Bankov, S. Becker, J. Triesch, P. J. Wild, and N. Flinner, "How to learn with intentional mistakes: NoisyEnsembles to overcome poor tissue quality for deep learning in computational pathology," *Frontiers Med.*, vol. 9, Aug. 2022, Art. no. 959068.

[37] N. Gnanavel, P. Inparaj, N. Sritharan, D. Meedeniya, and P. Yogarajah, "Interpretable cervical cell classification: A comparative analysis," in *Proc. 4th Int. Conf. Adv. Res. Comput. (ICARC)*, Feb. 2024, pp. 7–12, doi: 10.1109/ICARC61713.2024.10499737.

[38] L. Gamage, U. Isuranga, D. Meedeniya, S. De Silva, and P. Yogarajah, "Melanoma skin cancer identification with explainability utilizing mask guided technique," *Electronics*, vol. 13, no. 4, p. 680, Feb. 2024.

[39] T. Shyamalee, D. Meedeniya, G. Lim, and M. Karunarathne, "Automated tool support for glaucoma identification with explainability using fundus images," *IEEE Access*, vol. 12, pp. 17290–17307, 2024.

[40] N. Sritharan, N. Gnanavel, P. Inparaj, D. Meedeniya, and P. Yogarajah, "EnsembleCAM: Unified visualization for explainable cervical cancer identification," in *Proc. Int. Res. Conf. Smart Comput. Syst. Eng. (SCSE)*, vol. 7, Apr. 2024, pp. 1–6, doi: 10.1109/SCSE61872.2024.10550859.

[41] K. Kasture, "Ovarian cancer & subtypes," Mendeley Data, Tech. Rep., 2021, doi: 10.17632/kztymsrjx9.1.

[42] L. Alzubaidi, J. Zhang, A. J. Humaidi, A. Al-Dujaili, Y. Duan, O. Al-Shamma, J. Santamaría, M. A. Fadhel, M. Al-Amidie, and L. Farhan, "Review of deep learning: Concepts, CNN architectures, challenges, applications, future directions," *J. Big Data*, vol. 8, pp. 1–74, Mar. 2021, doi: 10.1186/s40537-021-00444-8.

[43] S. S. Tripathy, A. L. Imoize, M. Rath, N. Tripathy, S. Bebortta, C.-C. Lee, T.-Y. Chen, S. Ojo, J. Isabona, and S. K. Pani, "A novel edge-computing-based framework for an intelligent smart healthcare system in smart cities," *Sustainability*, vol. 15, no. 1, p. 735, Dec. 2022, doi: 10.3390/su150107 35.

[44] A. Khan, A. Sohail, U. Zahoora, and A. S. Qureshi, "A survey of the recent architectures of deep convolutional neural networks," *Artif. Intell. Rev.*, vol. 53, no. 8, pp. 5455–5516, Dec. 2020.

[45] S. Xie, R. Girshick, P. Dollár, Z. Tu, and K. He, "Aggregated residual transformations for deep neural networks," in *Proc. IEEE Conf. Comput. Vis. Pattern Recognit. (CVPR)*, Jul. 2017, pp. 5987–5995.

[46] K. Simonyan and A. Zisserman, "Very deep convolutional networks for large-scale image recognition," 2014, *arXiv:1409.1556*.

[47] A. G. Howard, M. Zhu, B. Chen, D. Kalenichenko, W. Wang, T. Weyand, M. Andreetto, and H. Adam, "MobileNets: Efficient convolutional neural networks for mobile vision applications," 2017, *arXiv:1704.04861*.

[48] K. He, X. Zhang, S. Ren, and J. Sun, "Deep residual learning for image recognition," in *Proc. IEEE Conf. Comput. Vis. Pattern Recognit. (CVPR)*, Jun. 2016, pp. 770–778.

[49] F. Chollet, "Xception: Deep learning with depthwise separable convolutions," in *Proc. IEEE Conf. Comput. Vis. Pattern Recognit. (CVPR)*, Jul. 2017, pp. 1251–1258.

[50] B. Koonce, *Convolutional Neural Networks With Swift for TensorFlow*. Berkeley, CA, USA: Apress, 2021, doi: 10.1007/978-1-4842-6168-2.

[51] C. Szegedy, W. Liu, Y. Jia, P. Sermanet, S. Reed, D. Anguelov, D. Erhan, V. Vanhoucke, and A. Rabinovich, "Going deeper with convolutions," in *Proc. IEEE Conf. Comput. Vis. Pattern Recognit. (CVPR)*, Jun. 2015, pp. 1–9.

[52] A. Singh, S. Sengupta, and V. Lakshminarayanan, "Explainable deep learning models in medical image analysis," *J. Imag.*, vol. 6, no. 6, p. 52, Jun. 2020.

[53] P. A. Bukłaho, J. Kiśluk, N. Wasilewska, and J. Nikliński, "Molecular features as promising biomarkers in ovarian cancer," *Adv. Clin. Exp. Med.*, vol. 32, no. 9, pp. 1029–1040, 2023.

[54] A. BenTaieb, H. Li-Chang, D. Huntsman, and G. Hamarneh, "Automatic diagnosis of ovarian carcinomas via sparse multiresolution tissue representation," in *Proc. 18th Int. Conf. Med. Image Comput. Comput.-Assist. Intervent. (MICCAI)*. Munich, Germany: Springer, Oct. 2015, pp. 629–636.

[55] A. BenTaieb, M. S. Nosrati, H. Li-Chang, D. Huntsman, and G. Hamarneh, "Clinically-inspired automatic classification of ovarian carcinoma subtypes," *J. Pathol. Informat.*, vol. 7, no. 1, p. 28, Jan. 2016.

[56] S. E. Kalloger, P. M. Baker, C. A. Ewanowich, J. Arseneau, V. Zherebitskiy, S. Abdulkarim, S. Leung, M. A. Duggan, D. Fontaine, R. Parker, D. G. Huntsman, and C. B. Gilks, "Diagnosis of ovarian carcinoma cell type is highly reproducible: A transcanadian study," *Amer. J. Surgical Pathol.*, vol. 34, no. 7, pp. 984–993, 2010.

[57] A. BenTaieb, H. Li-Chang, D. Huntsman, and G. Hamarneh, "A structured latent model for ovarian carcinoma subtyping from histopathology slides," *Med. Image Anal.*, vol. 39, pp. 194–205, Jul. 2017.

[58] M. Wu, C. Yan, H. Liu, and Q. Liu, "Automatic classification of ovarian cancer types from cytological images using deep convolutional neural networks," *Biosci. Rep.*, vol. 38, no. 3, Jun. 2018, Art. no. BSR20180289.

[59] A. B. Levine et al., "Synthesis of diagnostic quality cancer pathology images by generative adversarial networks," *J. Pathol.*, vol. 252, no. 2, pp. 178–188, Oct. 2020.

[60] K. R. Kasture, "A new deep learning method for automatic ovarian cancer prediction & subtype classification," *Turkish J. Comput. Math. Educ.*, vol. 12, no. 12, pp. 1233–1242, 2021.
[61] J. Boschman, H. Farahani, A. Darbandsari, P. Ahmadvand, A. Van Spankeren, D. Farnell, A. B. Levine, J. R. Naso, A. Churg, S. J. Jones, S. Yip, M. Köbel, D. G. Huntsman, C. B. Gilks, and A. Bashashati, "The utility of color normalization for AI-based diagnosis of hematoxylin and eosin-stained pathology images," *J. Pathol.*, vol. 256, no. 1, pp. 15–24, Jan. 2022.

MEERA RADHAKRISHNAN received the B.E. degree from the Department of Biomedical Engineering, Mahatma Gandhi Mission College of Engineering and Technology (MGMCET), Mumbai, under the University of Mumbai. She is currently pursuing the M.Tech. degree in medical informatics with the Department of Biomedical Engineering, Manipal Institute of Technology, Manipal. Her academic journey includes presentations at two international conferences, namely IEEE APSCON and ICCMEH. Notably, her paper from the 2024 IEEE Applied Sensing Conference (APSCON) has been successfully published. With a profound interest in research, she focuses on classification, prediction, and segmentation tasks across various health domains.

NIRANJANA SAMPATHILA (Senior Member, IEEE) received the B.E. degree in electronics and engineering and the M.Tech. degree in biomedical engineering from Mangalore University and the Ph.D. degree from Manipal University (currently known as Manipal Academy of Higher Education), Manipal, India. He is currently a Professor and the Head of the Department of Biomedical Engineering, Manipal Institute of Technology, Manipal Academy of Higher Education. He has more than 27 years of experience in research and academics in healthcare applications/biomedical engineering/electronics and communication engineering. He has published a good number of papers in journals and conferences. His research interests include pattern recognition, medical informatics, miniaturized system design, nanoelectronics, and AI for healthcare. He is associated with IEEE EMBS, Bengaluru Section.

H. MURALIKRISHNA received the B.E. degree from Visvesvaraya Technological University, Karnataka, India, in 2009, the M.Tech. degree in digital electronics and communication from Manipal Institute of Technology, Manipal, India, in 2013, and the Ph.D. degree from the School of Computing and Electrical Engineering, Indian Institute of Technology Mandi, Himachal Pradesh, India, in 2023. He is currently an Assistant Professor with the Department of Electronics and Communication Engineering, Manipal Institute of Technology, Manipal Academy of Higher Education, Manipal. His research interests include machine learning and deep learning, with applications in speech technology and biomedical signal processing.

K. S. SWATHI received the B.A.M.S. degree from Kuvempu University, and the M.B.A. degree in healthcare management and the Ph.D. degree from Manipal Academy of Higher Education, Manipal, India. She is an Associate Professor with the Department of Social and Health Innovation, Prasanna School of Public Health, Manipal Academy of Higher Education. She has more than 12 years of experience in research and academics in healthcare management and administration. She has published a good number of research papers in journals and conferences. Her research interests include health services management, quality management in healthcare, and digital health.